

Plausible presence of quark matter in neutron stars with masses above $0.97M_{\text{TOV}}$

Ming-Zhe Han,^{1,2} Yong-Jia Huang,^{1,2,3} Shao-Peng Tang,¹ and Yi-Zhong Fan^{1,2,*}

¹*Key Laboratory of Dark Matter and Space Astronomy, Purple Mountain Observatory, Chinese Academy of Sciences, Nanjing, 210033, People's Republic of China.*

²*School of Astronomy and Space Science, University of Science and Technology of China, Hefei, Anhui 230026, People's Republic of China.*

³*RIKEN Interdisciplinary Theoretical and Mathematical Sciences Program (iTHEMS), RIKEN, Wako 351-0198, Japan.*

(Dated: July 28, 2022)

Whether there is a quark matter core in the neutron star (NS) is a fundamental question. The increasing multi-messenger data set of NSs provide a valuable chance to examine such an attractive possibility. Here we carry out the Bayesian nonparametric inference of the NS equation of state (EOS) via a single-layer feed-forward neural network, taking into account the data of GW170817, PSR J0030+0451, and PSR J0740+6620, and incorporating the latest constraints from the chiral effective theory (χ EFT) and perturbative quantum chromodynamics (pQCD) at low and very high energy densities, respectively. It is found out that a sizable quark matter core ($\geq 10^{-3}M_{\odot}$) is plausible ($\geq 90\%$ probability) for the very massive NS with a gravitational mass above about $0.97M_{\text{TOV}}$, where M_{TOV} , the maximum gravitational mass of a non-rotating cold NS, is simultaneously constrained to be $2.18^{+0.27}_{-0.13}M_{\odot}$ (90% credibility). The average density of the quark matter core is found to be ~ 2.2 times that of the host NS. A few percent of the posterior EOSs, which do not predict quark matter cores even in the heaviest NSs, are characterized by a quicker rising of sound speed at relatively low densities. We also find that sound speed may reach close to zero near the center density of NS with $M \approx M_{\text{TOV}}$ and hence only allows the presence of the strong first-order phase transition in the center of the most massive NSs.

I. INTRODUCTION

The state of strongly interacting matter at exceedingly high density remains one of the long-standing open questions. Neutron star (NS), as it cools down the eons ahead after the birth in the supernova explosion, provides an astrophysical laboratory to investigate the dense, strongly interacting nuclear matter at zero temperature [1–3]. In the past five years, there have been some inspiring progress in astrophysical observations on NSs, including the multi-messenger observations of the first binary neutron star merger event GW170817 [4–7], the accurate mass determination of the very massive object PSR J0740+6620 (i.e., $M = 2.08 \pm 0.07M_{\odot}$ [8]), and the mass-radius measurements of PSR J0030+0451 and PSR J0740+6620 by the Neutron Star Interior Composition Explorer (NICER; [9–12]). These events/objects comprise the multi-messenger NS data set for our following analysis.

On the theoretical side, state-of-the-art ab-initio calculation provides precise boundary conditions for both low and high-density regimes. Currently, calculations using the chiral effective theory (χ EFT) have been achieved with incredibly high precision (the Next-to-Next-to-Next leading order, $N^3\text{LO}$) for many-body interactions [13]. Thus, the dense matter EOS up to $1.1\rho_{\text{sat}}$ is solidly constrained by the $N^3\text{LO}$ χ EFT calculations. Though the perturbative quantum chromodynamics (pQCD) is only valid at ultra-high density ($\geq 40\rho_{\text{sat}}$ [14]), the high-order pQCD calculation still provides a reference to the non-

perturbative effect at a lower density, with the chemical potential reaching 2.6 GeV, where its missing-higher-order (MHO) truncation error in pQCD is comparable with the uncertainty from χ EFT at $1.1\rho_{\text{sat}}$ [15]. Such a boundary constraint from pQCD can be pushed to a considerably lower density by causality, even reachable in astrophysical NSs [16]. The information that emerged from various directions reveals that the EOSs, which follow the χ EFT constraint in the low density, are required to undergo a rapidly stiffening, possibly exceed the conformal limit ($c_s^2/c^2 \leq 1/3$) [17–20] to support a massive NS, where c_s is the speed of sound inside the NS, and c is the speed of light in vacuum. Subsequently, they must slow down (or tend to be soft) to satisfy the causality-driven constraint from pQCD. Therefore, with the EOS structure determined by taking into account the observational and theoretical constraints, two key questions might be answered: how the quark-hadron transition takes place [2, 21–28] and whether quark matter core exists in astrophysical NSs [29–31].

In this work, we incorporate the latest χ EFT and pQCD results/constraints in our Bayesian nonparametric inference of NS EOS represented by the feed-forward neural network (FFNN) expansion [32] and then apply such an inference to the current multi-messenger NS data set. Different from the literature that assumes some structures (e.g., bumps, dips, and kinks) in the square of sound speed c_s^2 through a parametric form (e.g., [33]), our nonparametric representation of EOS is model-agnostic and can directly/robustly extract the structure information from the observation data. We notice a bump in the reconstructed c_s^2 curve at densities of $2 - 4\rho_{\text{sat}}$, which is more rapid than that of many pure-hadron matter models and breaks the conformal limit at 90% credibility. Fol-

* Corresponding author: yzfan@pmo.ac.cn

lowing Ref. [30], we assume that quark matter presents when the polytropic index $\gamma \leq 1.75$ is continuously satisfied to asymptotic densities. Then we show that quark cores are plausible ($\geq 90\%$ probability) for the NSs heavier than $0.97M_{\text{TOV}}$, where $M_{\text{TOV}} = 2.18_{-0.13}^{+0.27} M_{\odot}$ (90% credibility) is the maximum mass of non-rotating NSs. On the other side, in our approach, a $\sim 10^{-3}M_{\odot}$ quark core is merely possible for the NSs heavier than $\sim 0.9M_{\text{TOV}}$. Consistently, a $c_s^2 \rightarrow 0$ only happens in the center of the heaviest NS. Therefore, a strong first-order phase transition is unlikely in the low-mass NSs.

II. METHODS

So far, many phenomenological methods have been proposed to represent the NS EOS, which can be generally divided into two categories: the parametric and non-parametric methods. The parametric methods mainly include the piecewise polytropes [36], the spectral expansion [37], and the c_s^2 based parameterizations [30, 33, 38]. While the nonparametric methods involve the Gaussian process [39] and the feed-forward neural network (FFNN) expansion [32]. In this work, we use a nonparametric functional form of the $c_s^2(\rho)$ enhanced from Han *et al.* [32] to represent the EOS. The $c_s^2(\rho)$ can be described by a single-layer FFNN, i.e.,

$$c_s^2(\rho) = c^2 S\left(\sum_i^N w_{2i} \sigma(w_{1i} \ln(\rho) + b_{1i}) + b_2\right), \quad (1)$$

where w_{1i} , w_{2i} , b_{1i} , and b_2 are parameters (weights/bias) of the FFNN, N is the number of the nodes, and σ is a nonlinear function called activation function.

In this work, we still use the 10-node single-layer FFNN since it was found to be able to fit almost all theoretical EOSs pretty well [32]. And we consider two types of activation functions ($\sigma(x)$), *sigmoid* ($S(x)$) and *hyperbolic tangent* ($\tanh(x)$), which are defined as

$$S(x) = \frac{1}{1 + e^{-x}}, \quad (2)$$

$$\tanh(x) = \frac{e^x - e^{-x}}{e^x + e^{-x}}. \quad (3)$$

The model with $S(x)$ is easier to mimic the behavior of the hadronic EOS (with monotonously increasing sound speed) and the quark-hadron-crossover (QHC) EOS [27] with a gentle bump, while the model with $\tanh(x)$ is easier to generate the EOS like the first-order phase transition (with sound speed closed to zero at some density), or the QHC EOS with a sharp peak (see the Appendix A for the details). Therefore we use both of these two activation functions and combine these results (each result is obtained by the Bayesian inference separately). We match the constructed EOS in the NS crust density [40, 41], up to $\sim 0.3 \rho_{\text{sat}}$. From $0.3 \rho_{\text{sat}}$ to $1.1 \rho_{\text{sat}}$, we follow the solid constraint from N³LO χ EFT calculation

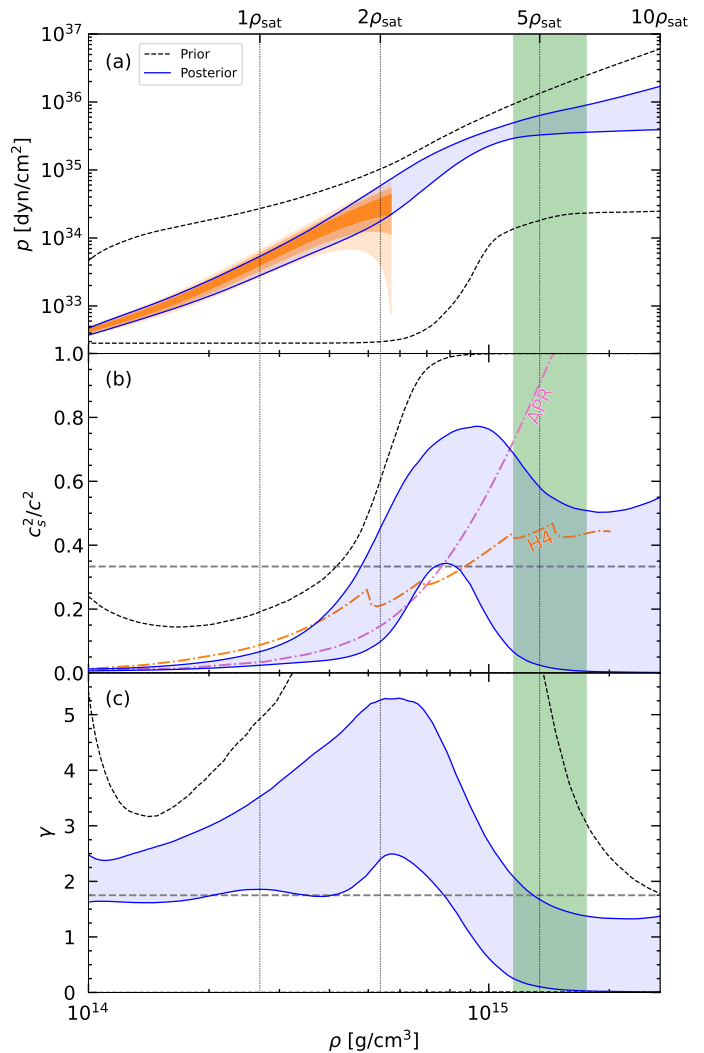


FIG. 1. The 90% credible intervals of the pressure p (panel (a)), the square of sound speed normalized by the square light speed c_s^2/c^2 (panel (b)) and γ (panel (c), $\gamma \equiv d(\ln p)/d(\ln \epsilon)$, where ϵ is the energy density.) v.s. rest-mass density. In all panels, the vertical dotted lines mark several nuclear densities and the green vertical region denotes the central density of the heaviest NS. The blue regions represent the posteriors and the black dashed curves are the edge of the priors (note that in panels (b) and (c), the lower bounds of the priors are very close to zero). The orange regions with different transparencies in panel (a) are the 1, 2, and 3 σ credible intervals of the χ EFT truncation errors [13]. The horizontal dashed line in panel (b) is the so-called conformal limit, i.e., $c_s^2/c^2 \leq 1/3$, and the dash-dotted lines with different colors are the c_s^2/c^2 of two representative hadronic EOSs, i.e., APR [34] and H4 [35]. In panel (c) the horizontal dashed line represents $\gamma = 1.75$.

[13]. At higher densities, it is expected that the uncertainty of the χ EFT calculation is not negligible. Therefore, we define the ρ_{ceft} as a variable in order to marginalize the χ EFT uncertainties from $1.1 \rho_{\text{sat}}$ to $2 \rho_{\text{sat}}$. We then uniformly sample ρ_{ceft} from $1.1 \rho_{\text{sat}}$ to $2 \rho_{\text{sat}}$ in the prior, where the density below ρ_{ceft} is thought valid to

be described by χ EFT calculation.

Once the EOS is constructed, we can then predict the relations between the macroscopic properties of NS, which can be used to perform the Bayesian inference to obtain the posterior distributions of the EOS given the observation data. The overall likelihood of the Bayesian inference can be expressed as

$$\mathcal{L} = \mathcal{L}_{\text{GW}} \times \mathcal{L}_{\text{NICER}} \times \mathcal{L}_{\chi\text{EFT}} \times \mathcal{L}_{\text{pQCD}}. \quad (4)$$

This likelihood consists of the following parts:

- $\mathcal{L}_{\text{GW}} = \mathcal{P}(m_1, m_2, \Lambda_1(m_1, \theta_{\text{EOS}}), \Lambda_2(m_1, \theta_{\text{EOS}}))$ is the marginalized likelihood of the GW170817 interpolated by the random forest [42], where $m_{1,2}$ and $\Lambda_{1,2}$ are the mass and tidal deformabilities of the primary/secondary NS in GW170817, and θ_{EOS} is the set of FFNN parameters, i.e., the weights and bias.
- $\mathcal{L}_{\text{NICER}} = \prod_i \mathcal{P}_i(M(\theta_{\text{EOS}}, h_i), R(\theta_{\text{EOS}}, h_i))$ is the likelihood of the NICER observations, where M , R , and h are the mass, radius, and core pseudo-enthalpy [43, 44] of the NS, respectively. We use the Gaussian kernel density estimation (KDE) of the public posterior samples of the data from two observations, PSR J0030+0451 [9, 10] and PSR J0740+6620 [11, 12] (for both observations we only use the data of Reily *et al.*).
- $\mathcal{L}_{\chi\text{EFT}} = \mathcal{P}(\epsilon, p, \rho_{\text{ceft}}, \theta_{\text{EOS}})$ is the likelihood considering the N^3LO calculation results of the χ EFT theory, where the ρ_{ceft} is a parameter of the Bayesian inference controlling the range of the χ EFT's implementation, the ϵ and p are energy density and pressure, respectively. We use the publicly available samples provided in [Github](#) of Drischler *et al.* [45] to obtain the means and standard deviations of the pressure. Then we define the $\mathcal{L}_{\chi\text{EFT}}$ as 1 only if the constructed EOS falls into the 3σ interval of the pressure, otherwise as 0.
- $\mathcal{L}_{\text{pQCD}} = \mathcal{P}(\rho_0, \epsilon(\rho_0, \theta_{\text{EOS}}), p(\rho_0, \theta_{\text{EOS}}))$ is the likelihood of implementing the pQCD constraints at high densities ($\sim 40\rho_{\text{sat}}$), where the ρ_0 is the rest-mass density of the last point of the constructed EOS, the ϵ and p are the corresponding energy density and pressure. As for the implementation of the likelihood, we use the public code released on [Github](#) [15, 46, 47].

The priors of the parameters in FFNN are set as the same as Han *et al.* [32], i.e., all the parameters of the FFNN are uniformly sampled in $(-5, 5)$. We use the Bayesian inference library BILBY [48] with the sampling algorithm PYMULTINEST to obtain the posterior samples of the EOSs. The EOS with M_{TOV} falling out of $(1.4, 3) M_{\odot}$ is discarded during the inference.

III. RESULTS AND DISCUSSIONS

As shown in the panel (a) of Fig. 1, the EOSs below the density of $\rho \sim 1.1\rho_{\text{sat}}$ are well constrained. This is anticipated since the χ EFT theory sets a tight constraint in this range; the sound speed thus lies on the low-value region of the priors. While in the middle region, there is a rapid increase of c_s^2 and the conformal limit has been violated at the 90% credibility. As a reference, the APR EOS with $R_{1.4} = 11.35\text{km}$ and H4 EOS with $R_{1.4} = 13.69\text{km}$ [9, 10] are also shown in panel (b) of Fig. 1, where $R_{1.4}$ denotes the radius of a $1.4M_{\odot}$ NS (as shown in Fig. 7, in our approach we have $R_{1.4} = 12.42^{+0.78}_{-1.06}$ km; the constraints on some other parameters are shown in Fig. 8). The rapid stiffening in the medium density, identified in a model-agnostic way, is a natural result required by the observations of NSs with a mass of $\sim 2M_{\odot}$. After that, the c_s^2 are suppressed in the high-density region ($\gtrsim 4\rho_{\text{sat}}$), as a consequence of the inclusion of the pQCD likelihood. Therefore, within the pQCD constraint, the hadronic EOS with a monotonously increasing sound speed is disfavored in the high-density region.

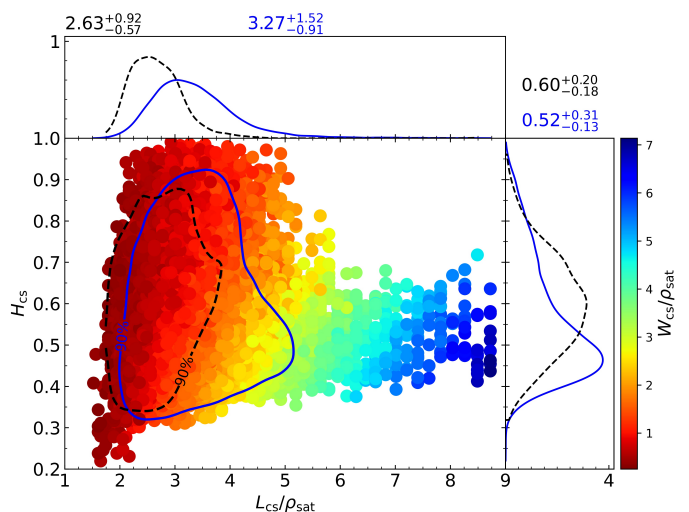


FIG. 2. The properties of c_s^2 peaks of the posterior EOSs. L_{cs} , H_{cs} , and W_{cs} are the location, the maximum value, and the half-width of the c_s^2 peak, respectively. The $W_{\text{cs}} > 0$ is defined as the difference between the L_{cs} and the position at the half height of H_{cs} . The solid (dashed) line is for all posterior EOSs (the EOSs without a quark matter core). The contours correspond to 90% credible regions, and all of the uncertainties of the reported values are also at the 90% credible level. And the one-dimensional plots are the probability density functions (PDFs).

The behavior of c_s^2 is impacted by many factors: the χ EFT in the low-density region constrains the initial condition of the sound speed, while the observed heavy NSs ($\gtrsim 2M_{\odot}$) and the pQCD information govern the peak's shape of the sound speed. A peak in the c_s^2 curve is quite common in our posterior EOSs. To describe the peak

structures more quantitatively, we characterize the peak of each EOS c_s^2 curve with its location, height, and width. In particular, we define the height of peak H_{cs} as the maximum c_s^2/c^2 of a specific EOS and the corresponding density as the location (i.e., L_{cs}). We measure the rapidness of the c_s^2 growth by its width $W_{cs} = L_{cs} - L_{hcs}$, where L_{hcs} represents the density when the c_s^2 reaches the half of its maximum (before the peak). The smaller the W_{cs} is, the more rapidly the sound speed grows. As shown in Fig. 2, the 90% confidence region is covered by blue contour, with $L_{cs} = 3.27^{+1.52}_{-0.91}\rho_{sat}$ and $H_{cs} = 0.53^{+0.30}_{-0.14}$, respectively. There is a strong positive correlation between W_{cs} and L_{cs} , suggesting that L_{hcs} is very close to L_{cs} in most cases. The red dots do not appear for $L_{cs} \geq 5\rho_{sat}$, implying that the rapid stiffening process at a rather high density is not permitted by the observation data. Some previous works have pointed out that the pressure at around $2\rho_{sat}$ strongly correlates with the radius of $\sim 1.4M_\odot$ canonical NS [49]. Therefore, a late stiffening will make it hard to achieve the pressure required by the radius measurements.

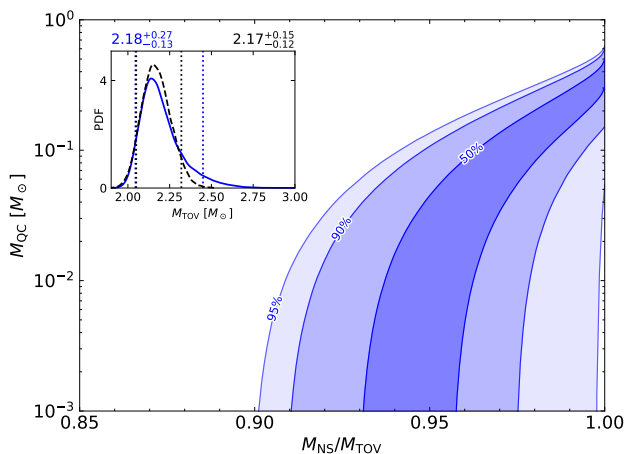


FIG. 3. Mass of the quark matter core versus the mass of an NS normalized to M_{TOV} for a given EOS (i.e., M_{NS}/M_{TOV}). The blue with different transparency represents the 50%, 90%, and 95% (2σ) credible regions, respectively. The insert presents the PDFs of the inferred M_{TOV} , where the result of this work is shown in solid blue line, and the dashed black line is taken from Fan *et al.* [50]. The uncertainty of the reported value is for the 90% credibility.

At sufficiently high density, fundamental theory predicts a hadron-quark transition [2]. To examine whether there is a quark matter core inside the NS and estimate its size, we employ the criterion of the polytropic index $\gamma \equiv d(\ln p)/d(\ln \epsilon) \leq 1.75$ [30] to calculate the size and mass of the quark core for each EOS. As seen from panel (c) of Fig. 1, the condition $\gamma \gtrsim 1.6$ is satisfied in density lower than $2\rho_{sat}$ (90% credible interval), which is consistent with the systematic study for γ of hadronic EOSs mentioned in [30]. Moreover, a quark matter core pos-

sibly presents inside the massive neutron star. Because the density where γ drops back to 1.75 could be lower than the center density of the NS with $M = M_{TOV}$.

Quantitatively, as shown in Fig. 3, under the condition that the quark matter appears, the mass of the quark core (M_{QC}) is sensitively dependent on the NS mass normalized by the corresponding M_{TOV} , i.e., M_{NS}/M_{TOV} . Moreover, no quark matter core is predicted for the NSs with masses below $\sim 0.9M_{TOV}$. While for $M_{NS} \approx M_{TOV}$, the 2σ (97.7%) ($\approx 90\%$ if we require more strictly that $\gamma \leq 1.5$; see Fig. 10) lower limit on the mass of the quark matter core is $\sim 10^{-3}M_\odot$. Moreover, now the maximum mass of a non-rotating NS is constrained to be $M_{TOV} = 2.18^{+0.27}_{-0.13} M_\odot$ (90% credibility), which is well consistent with that inferred with the data of GW170817/GRB 170817/AT2017gfo (i.e., $2.17^{+0.15}_{-0.12}M_\odot$ in the 90% credible interval [50]) by assuming that the central compact collapsed into a black hole at $t \sim 0.8$ s after the merger. Our result is thus in support of the black hole central engine model for GRB 170817A (see also [15]).

In the presence of a quark matter core, we normalize the mass and radius of such the strange heart to that of the host NS (i.e., M_{QC}/M_{NS} and R_{QC}/R_{NS}) and find an interesting “universal” relation (as shown in Fig. 4, most of the curves are concentrated in a narrow region). We fit the data with the function of $M_{QC}/M_{NS} = k(R_{QC}/R_{NS})^3$ and have $k = 2.16^{+0.27}_{-0.29}$ (90% credibility; see Fig. 9), suggesting that the average density of the quark matter core is ~ 2.2 times that of its host NS. Nevertheless, we would like to remind that in a few percent of the posterior EOSs, there is no evidence for the quark matter onset (i.e., $\gamma \leq 1.75$ criterion is not satisfied inside the heaviest NS). Such EOSs are characterized by their smaller L_{cs} and somewhat larger H_{cs} compared to those hosting strange hearts.

IV. SUMMARY

In this work, we adopt the Bayesian nonparametric method introduced in Han *et al.* [32] to constrain the EOSs and study the sound speed properties of NS matter. We incorporate the state-of-the-art χ EFT results up to $\sim 1.1\rho_{sat}$ in the low-density range and implement the pQCD likelihood at high density. Therefore, our nonparametric representation method can effectively generate various EOSs that satisfy the fundamental nuclear physics constraints. Then, we use the mass–tidal-deformability measurements of GW170817 and the mass–radius of PSR J0030+0451/PSR J0740+6620 measured by NICER to perform Bayesian inference of EOS. The sound speed properties reconstructed from the posteriors show that the maximum sound speed is above the so-called conformal limit NS at the 90% credible level. After tracking the structure of the c_s^2 curve for each EOS, we find a bump feature in most cases. Furthermore, such peak structure is found to be related to the rapid stiffening process,

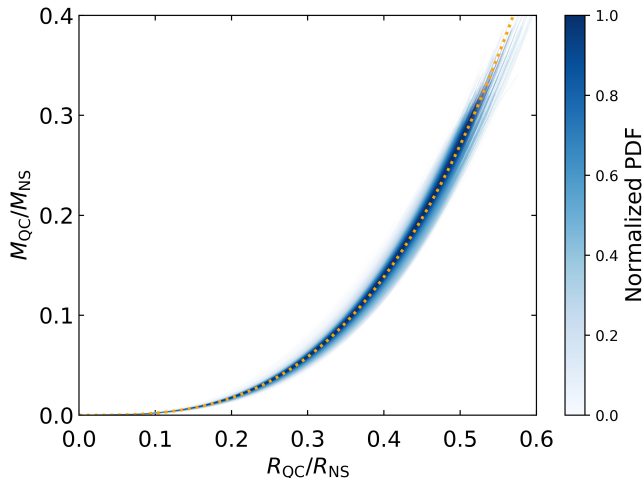


FIG. 4. The relation between mass and radius of the quark matter core normalized to those of the host NS. Each curve corresponds to an EOS from posteriors and is colored by its normalized PDF. The yellow dashed line represents the fit of $M_{\text{QC}}/M_{\text{NS}} = 2.16(R_{\text{QC}}/R_{\text{NS}})^3$.

and our results indicate that the earlier the rapid stiffening happens, the stronger it will be. Supposing the quark matter appears in the density region characterized by $\gamma \leq 1.75$, we show that for $M_{\text{NS}} = 0.97M_{\text{TOV}}$ a sizable quark matter core presents at 90% probability. In view of the inferred $M_{\text{TOV}} = 2.18_{-0.13}^{+0.27}M_{\odot}$ (90% credibility), PSR J0740+6620 may have a mass exceeding such a “threshold” and hence host a quark core with a probability of ≈ 0.52 (see the Appendix C for the details). The scientific O4 run of the LIGO/Virgo/KAGRA network [51] is upcoming this year and NICER will soon release more mass–radius measurement results. Therefore, more stringent constraints on the EOS will be set and the conclusions of this work will be verified/tested in the near future.

Acknowledgments. The authors thank O. Komoltsev for the help in implementing the pQCD likelihood, and J.L. Jiang, T. Kojo and T. Hatsuda for the useful discussions. This work was supported in part by NSFC under grants No. 11921003 and No. 11525313.

Appendix A: Choice of the activation functions

Here, we go into further detail on the techniques used in the main text. By use of a feed-forward neuron network (FFNN), we developed a nonparametric representation of the neutron star (NS) equation of state (EOS) in Han *et al.* [32]. In that work, the functional form of the NS EOS is constructed as

$$\phi(p) = \sum_i^N w_{2i} S(w_{1i} \ln(p) + b_{1i}) + b_2, \quad (\text{A1})$$

where w_{1i} , w_{2i} , b_{1i} , and b_2 are parameters (weights/bias), N is the number of nodes, $S(x)$ is the sigmoid function

$$S(x) = \frac{1}{1 + e^{-x}}, \quad (\text{A2})$$

p is the pressure, and ϕ is the auxiliary variable ensuring the microscopical stability and causality condition, i.e., $0 \leq c_s^2/c^2 \leq 1$, which is defined as

$$\phi = \log(c^2/c_s^2 - 1). \quad (\text{A3})$$

In this work, we extend the above model with some improvements, and the new version of EOS representation can be expressed as

$$c_s^2(\rho) = c^2 S\left(\sum_i^N w_{2i} \sigma(w_{1i} \ln(\rho) + b_{1i}) + b_2\right), \quad (\text{A4})$$

where ρ is the rest-mass density, c is the speed of light in vacuum, and $\sigma(x)$ is a nonlinear function called activation function. Here and after, we define

$$X_i = w_{1i} \ln(\rho) + b_{1i}, \quad (\text{A5})$$

$$Y = \sum_i^N w_{2i} \sigma(X_i) + b_2. \quad (\text{A6})$$

Noticed that if we take $\sigma(x) = x$, which is often called a linear activation, the functional form is very similar to the spectral expansion described in Lindblom [52], i.e.,

$$c_s^2(p) = c^2 \left\{ 1 + \exp \left[- \sum_k v_k \Phi_k(p) \right] \right\}, \quad (\text{A7})$$

where Φ_k is the basis function, and v_k is the corresponding coefficient. Therefore, the new model is more like a general extension of the spectral representation.

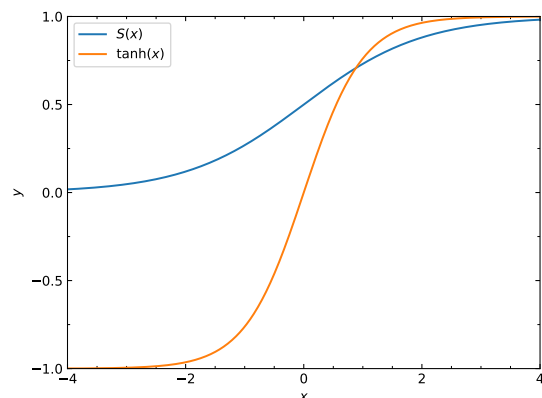


FIG. 5. Activation functions used in this work, i.e., *sigmoid* function $S(x)$ and *hyperbolic tangent* function $\tanh(x)$.

Meanwhile, we take two kinds of activation functions in the current work, i.e., $\sigma(x) = S(x)$ and $\sigma(x) = \tanh(x)$,

where $\tanh(x)$ is the *hyperbolic tangent* function. These two activation functions are displayed in Fig. 5, where we can see that both $S(x)$ and $\tanh(x) \rightarrow 1$ when $x \rightarrow +\infty$, while when $x \rightarrow -\infty$, $S(x) \rightarrow 0$ and $\tanh(x) \rightarrow -1$. Given the fixed parameters (w_{1i} , w_{2i} , b_{1i} , and b_2) (when a sample of these parameters is drawn from the prior), we find that $\tanh(X_i)$ changes more sharply than $S(X_i)$ as the independent variable (i.e., $\ln(\rho)$) changes. As a result, the Y with $\sigma(x) = \tanh(x)$ may be more easier to get away from zero than the Y with $\sigma(x) = S(x)$, which will in turn make the c_s^2/c^2 approaches 0 or 1. Therefore, *hyperbolic tangent* activation function could mimic the c_s^2 behaviors of the first-order phase transition ($c_s^2/c^2 \sim 0$), or a smooth quark-hadron crossover (QHC) with sharp peak ($c_s^2/c^2 \sim 1$). On the other hand, the model with *sigmoid* activation function prefers to generate the EOSs that asymptotically approach median c_s^2 . So it could generate the pure-hadron-like EOSs (with a monotonously increasing sound speed) or a QHC with a gentle bump. Combined with the two activation functions, the prior space would be large enough to include the general types of physical-motivated EOSs.

As shown in Fig. 6, we randomly select 500 EOSs from the prior, which could fill the space in c_s^2 after $\sim 2\rho_{\text{sat}}$. In particular, we mark four typical EOSs from *hyperbolic tangent* and *sigmoid* activation functions by dash-dotted and dashed lines, respectively. The possible physical clarification of them is marked with different colors. In practice, we perform the Bayesian inference separately with each activation function; all the priors of the parameters in the inference are the same except for the choice of the $\sigma(x)$. Then we combine the posteriors of the parameters to obtain the final results. Please note that what we discuss above is a preference of the EOSs' types the two activation functions could generate. We do not imply the models with *sigmoid* or *hyperbolic tangents* can only represent EOSs in a specific physical clarification.

Appendix B: General constraints for NS properties and EOS parameters

In addition to the constraints for the EOSs mentioned in the main text, we provide more information from our model-agnostic Bayesian inference. In Fig. 7, we reconstruct the 90% credible region for the mass-radius ($M-R$) constrained from the posterior samples. The remarkable observation of binary neutron star merger event GW170817 [6, 7], and two $M-R$ measurements of PSR J0030+0451 [9, 10] and PSR J0740+6620 [11, 12] are also shown. The joint information provides a better constraint, with $R_{1.4} = 12.42^{+0.78}_{-1.06}$ km and $R_{2.0} = 12.30^{+0.90}_{-1.11}$ km (90% credible interval).

Some additional quantities of interest with their possible correlations are presented in Fig. 8. The $\Lambda_{1.4}$ is the dimensionless tidal deformability (Λ) of a $1.4M_\odot$ NS, the Λ is defined as $\Lambda = (2/3)k_2[(c^2/G)(R/m)]^5$, where k_2 is the tidal Love number [53–56]. ρ_c , p_c , and $(c_s^2/c^2)_c$

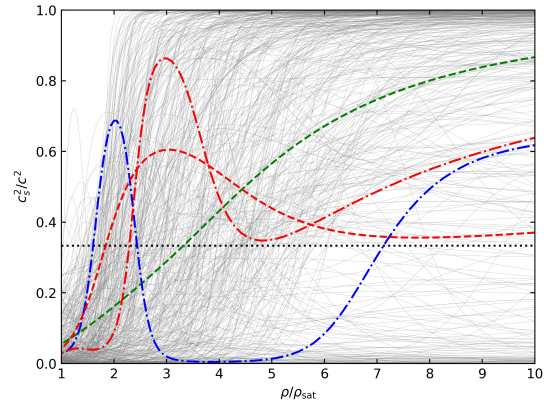


FIG. 6. Speed of sound (c_s^2/c^2) v.s. rest-mass density for the randomly selected 500 EOSs from the prior. Several types of physical-motivated EOSs, such as the hadronic (green, with monotonously increasing c_s^2/c^2), the first-order phase transition (blue, with c_s^2/c^2 close to zero at some density), the quark-hadron crossover (red, with a bump of $c_s^2/c^2 \geq 1/3$ and back to $c_s^2/c^2 \sim 1/3$ at ultra-high density ($\sim 40n_0$)) could be generated in our framework. The dashed and dash-dotted lines represent the samples generated by the model with a *sigmoid* activation function and the model with a *hyperbolic tangents* activation function, respectively.

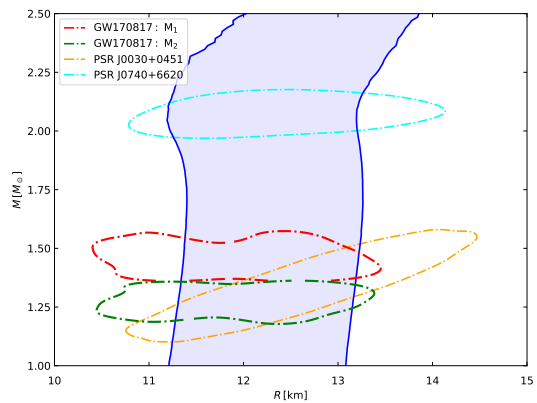


FIG. 7. The 90% credible region (blue shadowed area) of the $M-R$ relation. The dash-dotted contours (68% confidence level) in red, green, orange, and cyan are the mass-radius measurements of the primary, the secondary object of GW170817 (data taken from the right panel of Fig. 3 of Abbott *et al.* [6]), PSR J0030+0451, and PSR J0740+6620, respectively.

are the rest-mass density, pressure, and speed of sound normalized by light speed in the center of the NS with $M = M_{\text{TOV}}$, respectively. H_{cs} and L_{cs} are, as defined in the main text, the peak value of the sound speed and the location where the sound speed reaches its peak value. Finally, we also show a parameter that measures the difference between the radius of a $1.4M_\odot$ NS and $2.0M_\odot$

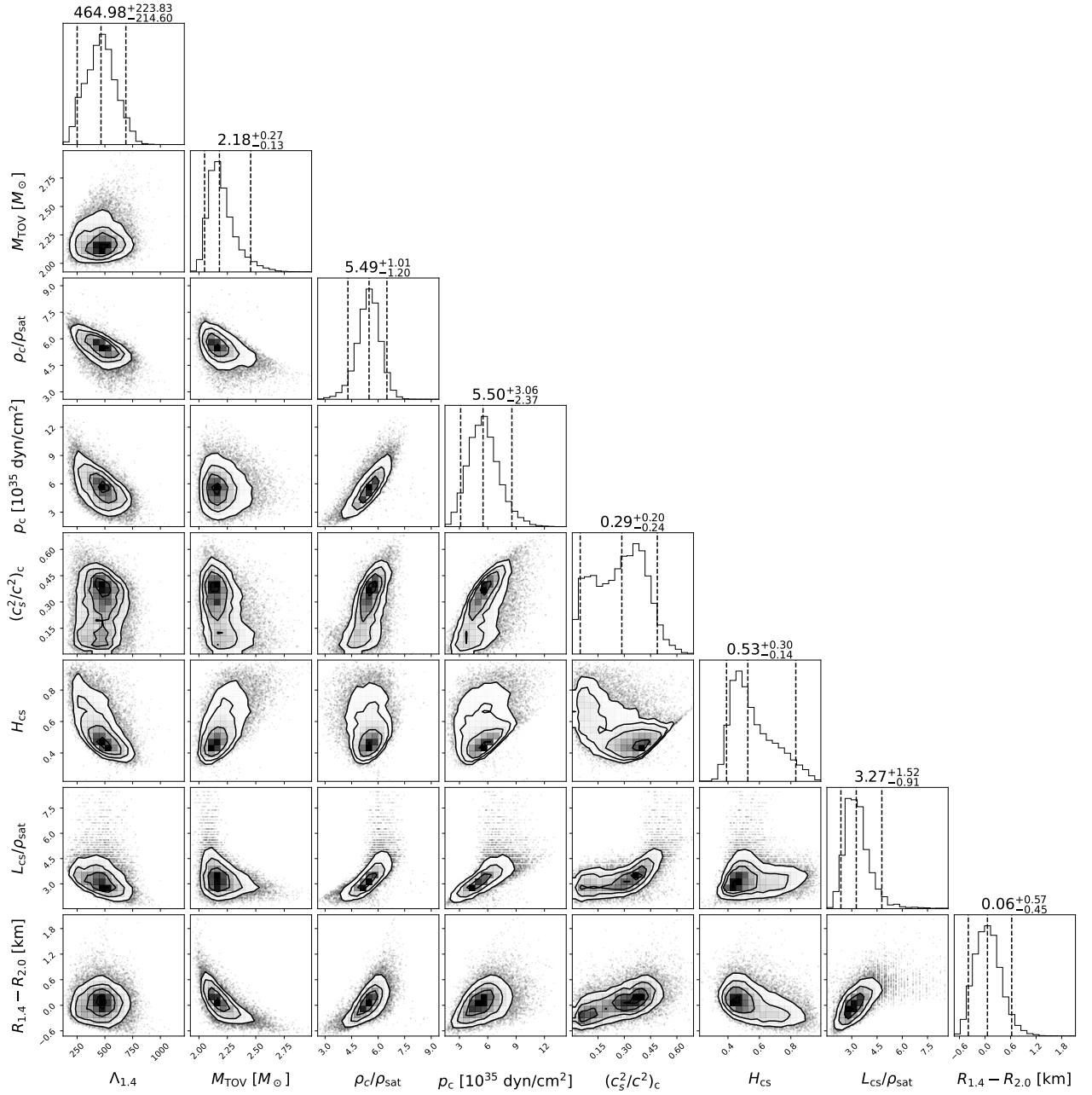


FIG. 8. Corner plots of the probability distributions for the tidal deformability of a canonical $1.4M_{\odot}$ NS ($\Lambda_{1.4}$), the maximum mass of a non-rotation NS (M_{TOV}), the rest-mass density, pressure, and sound speed in the center of the NS with $M = M_{\text{TOV}}$ (ρ_c , p_c , and $(c_s^2/c^2)_c$), the value of the peak in sound speed (H_{cs}), the location of the peak in sound speed (L_{cs}/ρ_{sat}), and the difference between the radii of a $1.4M_{\odot}$ and a $2.0M_{\odot}$ NSs ($R_{1.4} - R_{2.0}$) of the EOS posterior samples. The error bars/lines are all at the 90% credible level.

NS, i.e., $R_{1.4} - R_{2.0}$.

In Fig. 9 we show the probability density distribution of $k = (M_{\text{QC}}/M_{\text{NS}})/(R_{\text{QC}}/R_{\text{NS}})^3$, a coefficient that connects the average density of the quark matter core and that of the host NS, which we have defined in the main text.

Appendix C: Probability for PSR J0740+6620 hosting a quark core

In the main text, we have concluded that a sizable quark core is only plausible to be present in the very massive NS with a mass larger than $0.97M_{\text{TOV}}$. Such a value is obtained as follows: given a series of NS masses normalized by the corresponding M_{TOV} of

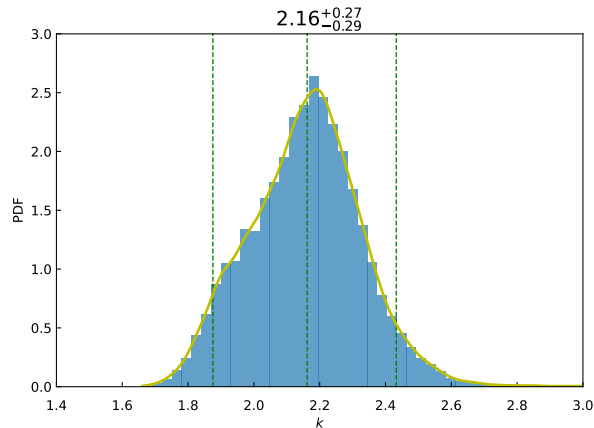


FIG. 9. Probability density function of the $k = (M_{\text{QC}}/M_{\text{NS}})/(R_{\text{QC}}/R_{\text{NS}})^3$, where $M_{\text{QC}}/R_{\text{QC}}$ are the mass/radius of the quark matter core, and $M_{\text{NS}}/R_{\text{NS}}$ are the mass/radius of its host NS.

each EOS, we calculate the ratio of EOSs that predict $M_{\text{QC}} > 10^{-3}M_{\odot}$ for each value of $M_{\text{NS}}/M_{\text{TOV}}$ (as shown in Fig. 10); then we can directly find the percentile where almost $> 90\%$ EOSs support that the NSs have quark matter cores larger than $10^{-3}M_{\odot}$. Based on the above results, it is pretty interesting to investigate whether (or how possible) the observed maximum mass NS PSR J0740+6620 hosts nonnegligible quark matters (e.g., $> 10^{-3}M_{\odot}$) inside its core. The 68.3% credible interval of $M_{\text{NS}}/M_{\text{TOV}}$ for PSR J0740+6620 is estimated to $0.971^{+0.022}_{-0.036}$ by reconstructing the posterior samples obtained in the Bayesian inference. To evaluate the overall chance for PSR J0740+6620 hosting a quark core, we marginalize the uncertainties of its mass measurement and the EOSs using

$$P = \sum_i^{N_{\text{EOS}}} \mathcal{P}(\text{EOS}_i) \frac{\int_{M_{\text{NS}}(M_{\text{QC}}=10^{-3}M_{\odot}|\text{EOS}_i)}^{M_{\text{TOV},i}} dm \mathcal{P}(m)}{\int_{-\infty}^{M_{\text{TOV},i}} dm \mathcal{P}(m)} \quad (\text{A1})$$

where $\mathcal{P}(m)$ is the mass distribution of PSR J0740+6620, $M_{\text{NS}}(M_{\text{QC}} | \text{EOS}_i)$ is the function between M_{NS} and M_{QC} given the i -th EOS in the posterior samples, and $M_{\text{TOV},i}$ is the corresponding maximum mass. Since our posterior samples are equal-weighted, $\mathcal{P}(\text{EOS}_i)$ can be simply taken as $1/N_{\text{EOS}}$, where N_{EOS} is the sample size. Finally, we find that PSR J0740+6620 has a probability of 52.5% for hosting a sizable quark core if we take the criteria of $\gamma < 1.75$ for the emergence of quark matter. Such a probability decreases to 24.5% when we change the criteria to $\gamma < 1.5$.

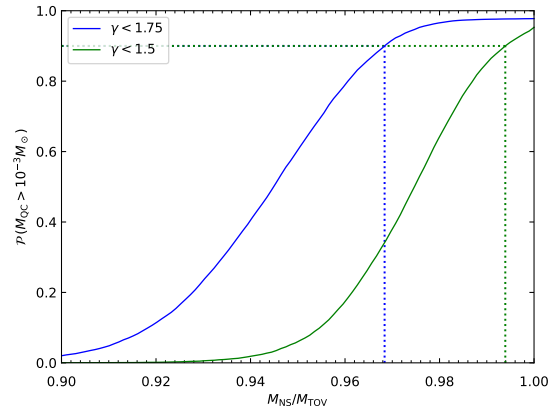


FIG. 10. Ratios of EOSs predicting $M_{\text{QC}} > 10^{-3}M_{\odot}$ as a function of the normalized masses $M_{\text{NS}}/M_{\text{TOV}}$. The dotted blue (green) lines mark the position where 90% EOSs give $10^{-3}M_{\odot}$ quark matter cores for the NSs with masses of $0.968M_{\text{TOV}}$ ($0.994M_{\text{TOV}}$), assuming the criteria of $\gamma < 1.75$ ($\gamma < 1.5$) for the onset of quark matter inside NSs.

- [1] M. Oertel, M. Hempel, T. Klöhn, and S. Typel, *Reviews of Modern Physics* **89**, 015007 (2017), arXiv:1610.03361 [astro-ph.HE].
- [2] G. Baym, T. Hatsuda, T. Kojo, P. D. Powell, Y. Song, and T. Takatsuka, *Reports on Progress in Physics* **81**, 056902 (2018).
- [3] J. M. Lattimer, *Ann. Rev. Nucl. Part. Sci.* **71**, 433 (2021).
- [4] B. P. Abbott, R. Abbott, T. D. Abbott, and et al. (LIGO Scientific Collaboration and Virgo Collaboration), *Phys. Rev. Lett.* **119**, 161101 (2017).
- [5] B. P. Abbott, R. Abbott, T. D. Abbott, and et al., *ApJ* **848**, L12 (2017), arXiv:1710.05833 [astro-ph.HE].
- [6] B. P. Abbott, R. Abbott, T. D. Abbott, and et al., *Phys. Rev. Lett.* **121**, 161101 (2018), arXiv:1805.11581 [gr-qc].
- [7] B. P. Abbott, R. Abbott, T. D. Abbott, and et al., *Physical Review X* **9**, 011001 (2019), arXiv:1805.11579 [gr-qc].
- [8] H. T. Cromartie, E. Fonseca, S. M. Ransom, and et al., *Nature Astronomy* **4**, 72 (2020), arXiv:1904.06759 [astro-ph.HE].
- [9] T. E. Riley, A. L. Watts, S. Bogdanov, and et al., *ApJ* **887**, L21 (2019), arXiv:1912.05702 [astro-ph.HE].
- [10] M. C. Miller, F. K. Lamb, A. J. Dittmann, and et al., *ApJ* **887**, L24 (2019), arXiv:1912.05705 [astro-ph.HE].
- [11] T. E. Riley, A. L. Watts, P. S. Ray, and et al., *ApJ* **918**, L27 (2021), arXiv:2105.06980 [astro-ph.HE].
- [12] M. C. Miller, F. K. Lamb, A. J. Dittmann, and et al., *ApJ* **918**, L28 (2021), arXiv:2105.06979 [astro-ph.HE].
- [13] C. Drischler, K. Hebeler, and A. Schwenk, *Phys. Rev. Lett.* **122**, 042501 (2019).
- [14] A. Kurkela, P. Romatschke, and A. Vuorinen, *Phys. Rev. D* **81**, 105021 (2010).
- [15] T. Gorda, O. Komoltsev, and A. Kurkela, arXiv e-prints, arXiv:2204.11877 (2022), arXiv:2204.11877 [nucl-th].
- [16] O. Komoltsev and A. Kurkela, *Phys. Rev. Lett.* **128**, 202701 (2022).
- [17] P. Bedaque and A. W. Steiner, *Phys. Rev. Lett.* **114**, 031103 (2015).
- [18] L. McLerran and S. Reddy, *Phys. Rev. Lett.* **122**, 122701 (2019).
- [19] K. S. Jeong, L. McLerran, and S. Sen, *Phys. Rev. C* **101**, 035201 (2020).
- [20] T. Kojo, *Phys. Rev. D* **104**, 074005 (2021).
- [21] E. R. Most, L. R. Weih, L. Rezzolla, and J. Schaffner-Bielich, *Phys. Rev. Lett.* **120**, 261103 (2018), arXiv:1803.00549 [gr-qc].
- [22] G. Montaña, L. Tolós, M. Hanauske, and L. Rezzolla, *Phys. Rev. D* **99**, 103009 (2019), arXiv:1811.10929 [astro-ph.HE].
- [23] S. Han and M. Prakash, *ApJ* **899**, 164 (2020), arXiv:2006.02207 [astro-ph.HE].
- [24] S.-P. Tang, J.-L. Jiang, W.-H. Gao, Y.-Z. Fan, and D.-M. Wei, *Phys. Rev. D* **103**, 063026 (2021), arXiv:2009.05719 [astro-ph.HE].
- [25] S.-P. Tang, J.-L. Jiang, M.-Z. Han, Y.-Z. Fan, and D.-M. Wei, *Phys. Rev. D* **104**, 063032 (2021), arXiv:2106.04204 [nucl-th].
- [26] K. Masuda, T. Hatsuda, and T. Takatsuka, *Astrophys. J.* **764**, 12 (2013).
- [27] G. Baym, S. Furusawa, T. Hatsuda, T. Kojo, and H. Togashi, *ApJ* **885**, 42 (2019), arXiv:1903.08963 [astro-ph.HE].
- [28] T. Kojo, *Phys. Rev. D* **104**, 074005 (2021).
- [29] J. M. Lattimer and M. Prakash, *Science* **304**, 536 (2004), arXiv:astro-ph/0405262 [astro-ph].
- [30] E. Annala, T. Gorda, A. Kurkela, J. Nättilä, and A. Vuorinen, *Nature Physics* **16**, 907 (2020), arXiv:1903.09121 [astro-ph.HE].
- [31] M. Ferreira, R. C. Pereira, and C. m. c. Providência, *Phys. Rev. D* **101**, 123030 (2020).
- [32] M.-Z. Han, J.-L. Jiang, S.-P. Tang, and Y.-Z. Fan, *ApJ* **919**, 11 (2021), arXiv:2103.05408 [hep-ph].
- [33] H. Tan, J. Noronha-Hostler, and N. Yunes, *Phys. Rev. Lett.* **125**, 261104 (2020), arXiv:2006.16296 [astro-ph.HE].
- [34] A. Akmal, V. R. Pandharipande, and D. G. Ravenhall, *Phys. Rev. C* **58**, 1804 (1998), arXiv:nucl-th/9804027 [nucl-th].
- [35] B. D. Lackey, M. Nayyar, and B. J. Owen, *Phys. Rev. D* **73**, 024021 (2006), arXiv:astro-ph/0507312 [astro-ph].
- [36] J. S. Read, B. D. Lackey, B. J. Owen, and J. L. Friedman, *Phys. Rev. D* **79**, 124032 (2009).
- [37] L. Lindblom and N. M. Indik, *Phys. Rev. D* **89**, 064003 (2014).
- [38] H. Tan, T. Dore, V. Dexheimer, J. Noronha-Hostler, and N. Yunes, *Phys. Rev. D* **105**, 023018 (2022), arXiv:2106.03890 [astro-ph.HE].
- [39] R. Essick, P. Landry, and D. E. Holz, *Phys. Rev. D* **101**, 063007 (2020).
- [40] G. Baym, C. Pethick, and P. Sutherland, *Astrophys. J.* **170**, 299 (1971).
- [41] F. Douchin and P. Haensel, *A&A* **380**, 151 (2001), arXiv:astro-ph/0111092 [astro-ph].
- [42] F. Hernandez Vivanco, R. Smith, E. Thrane, and P. D. Lasky, *MNRAS* **499**, 5972 (2020), arXiv:2008.05627 [astro-ph.HE].
- [43] L. Lindblom and N. M. Indik, *Phys. Rev. D* **86**, 084003 (2012), arXiv:1207.3744 [astro-ph.HE].
- [44] L. Lindblom and N. M. Indik, *Phys. Rev. D* **89**, 064003 (2014), arXiv:1310.0803 [astro-ph.HE].
- [45] C. Drischler, R. J. Furnstahl, J. A. Melendez, and D. R. Phillips, *Phys. Rev. Lett.* **125**, 202702 (2020), arXiv:2004.07232 [nucl-th].
- [46] T. Gorda, A. Kurkela, R. Paatelainen, S. Säppi, and A. Vuorinen, *Phys. Rev. Lett.* **127**, 162003 (2021), arXiv:2103.05658 [hep-ph].
- [47] O. Komoltsev and A. Kurkela, *Phys. Rev. Lett.* **128**, 202701 (2022), arXiv:2111.05350 [nucl-th].
- [48] G. Ashton, M. Hübner, P. D. Lasky, C. Talbot, K. Ackley, S. Biscoveanu, Q. Chu, A. Divakarla, P. J. Easter, B. Goncharov, F. Hernandez Vivanco, J. Harms, M. E. Lower, G. D. Meadors, D. Melchor, E. Payne, M. D. Pitkin, J. Powell, N. Sarin, R. J. E. Smith, and E. Thrane, *ApJS* **241**, 27 (2019), arXiv:1811.02042 [astro-ph.IM].
- [49] J. M. Lattimer and M. Prakash, *ApJ* **550**, 426 (2001), arXiv:astro-ph/0002232 [astro-ph].
- [50] Y.-Z. Fan, J.-L. Jiang, S.-P. Tang, Z.-P. Jin, and D.-M. Wei, *ApJ* **904**, 119 (2020), arXiv:2005.10482 [astro-ph.HE].
- [51] B. P. Abbott, R. Abbott, T. D. Abbott, and et al., *Living Reviews in Relativity* **23**, 3 (2020).

- [52] L. Lindblom, *Phys. Rev. D* **82**, 103011 (2010), [arXiv:1009.0738 \[astro-ph.HE\]](#).
- [53] T. Hinderer, *ApJ* **677**, 1216 (2008), [arXiv:0711.2420 \[astro-ph\]](#).
- [54] É. É. Flanagan and T. Hinderer, *Phys. Rev. D* **77**, 021502 (2008), [arXiv:0709.1915 \[astro-ph\]](#).
- [55] T. Damour and A. Nagar, *Phys. Rev. D* **80**, 084035 (2009), [arXiv:0906.0096 \[gr-qc\]](#).
- [56] T. Binnington and E. Poisson, *Phys. Rev. D* **80**, 084018 (2009), [arXiv:0906.1366 \[gr-qc\]](#).